



ELSEVIER

Available online at www.sciencedirect.com

SCIENCE @ DIRECT®

Journal of Magnetism and Magnetic Materials 260 (2003) 273–281

www.elsevier.com/locate/jmmm

Dependence of exchange bias in $\text{Ni}_{81}\text{Fe}_{19}/\text{Pt}_x\text{Mn}_{1-x}$ ($0 < x < 0.2$) bilayers on composition and microstructure

Haiwen Xi*, Bo Bian, Keith R. Mountfield, Zailong Zhuang,
David E. Laughlin, Robert M. White

Data Storage Systems Center, Carnegie Mellon University, Pittsburgh, PA 15213, USA

Received 18 December 2001

Abstract

The exchange coupling between ferromagnetic $\text{Ni}_{81}\text{Fe}_{19}$ and antiferromagnetic $\text{Pt}_x\text{Mn}_{1-x}$ films prepared by RF magnetron sputtering has been investigated. The study has focused on the relationship between the exchange bias and the structural characteristics of the $\text{Pt}_x\text{Mn}_{1-x}$ films, such as crystallinity, texture, and granularity. The Pt content of the $\text{Pt}_x\text{Mn}_{1-x}$ film is in the range of 0 at% $< x < 20$ at%. The exchange bias in this system is associated with the stabilization of the γ -phase with a disordered FCC structure in the $\text{Pt}_x\text{Mn}_{1-x}$ films. Although the texture of the polycrystalline $\text{Pt}_x\text{Mn}_{1-x}$ films improves with increasing Pt content, a relatively large exchange field of 64 Oe at room temperature and a high blocking temperature of about 200°C were found in $\text{Ni}_{81}\text{Fe}_{19}$ (15 nm)/ $\text{Pt}_8\text{Mn}_{92}$ (30 nm). The exchange bias of the $\text{Ni}_{81}\text{Fe}_{19}/\text{Pt}_x\text{Mn}_{1-x}$ bilayers is dependent on the intrinsic properties of the $\text{Pt}_x\text{Mn}_{1-x}$ films, such as the exchange coupling between the antiferromagnetic moments and the magnetocrystalline anisotropy, which decrease with the Pt doping concentration.

© 2002 Published by Elsevier Science B.V.

PACS: 75.70.Cn; 75.30.Gw; 75.60.Ej; 75.50.Ss

Keywords: Exchange bias; Ferromagnetic/antiferromagnetic coupling; Biasing materials; PtMn; Magnetic thin film

1. Introduction

Extensive studies have been made on exchange biasing materials for their application in anisotropic magnetoresistive (AMR) and giant magnetoresistive (GMR) spin-valve sensors used in high-density recording. Antiferromagnetic (AF) FeMn was originally used for domain stabiliza-

tion in AMR sensors [1]. In addition to FeMn, other exchange materials, such as CoNiO, NiMn, IrMn, CrMnPt and RuRhMn, have been investigated [2–8]. However, little work has been done on the AF PtMn alloy with less than 20 at% Pt content [9,10]. We have investigated exchange biasing between ferromagnetic (FM) $\text{Ni}_{81}\text{Fe}_{19}$ and AF $\text{Pt}_x\text{Mn}_{1-x}$ ($0 \text{ at\%} < x < 20 \text{ at\%}$) films. In this article, magnetic properties, electrical resistivity, thermal stability, texture and microstructure of the exchange-biased bilayers will be presented.

*Corresponding author. Recording Head Operations, Seagate Technology, Bloomington, MN, 55435 USA.

E-mail address: haiwen.Xi@seagate.com (H. Xi).

2. Experimental

$\text{Ni}_{81}\text{Fe}_{19}/\text{Pt}_x\text{Mn}_{1-x}$ ($0 \text{ at}\% < x < 20 \text{ at}\%$) bilayers were sequentially deposited by RF magnetron sputtering onto glass substrates with a Ta buffer layer in a homemade five target sputtering system. Another 5 nm Ta layer was deposited on top of the $\text{Pt}_x\text{Mn}_{1-x}$ layer to protect samples against oxidation in air. The base pressure of the system was typically 10^{-7} Torr. The $\text{Ni}_{81}\text{Fe}_{19}$ film was sputtered from a permalloy target at an Ar pressure of 4 mTorr and a supply power of 400 W. The $\text{Pt}_x\text{Mn}_{1-x}$ films were sputtered from a Mn target with Pt chips bonded to it. Exchange biasing, first observed in the $\text{Ni}_{81}\text{Fe}_{19}/\text{Pt}_x\text{Mn}_{1-x}$ bilayer films with about 10 at% Pt content, is strongly dependent on the deposition conditions. The deposition condition dependence of the exchange biasing has been reported earlier [10]. All $\text{Pt}_x\text{Mn}_{1-x}$ films were deposited at the optimized conditions of 20 mTorr and 100 W. Exchange bias can be obtained in as-deposit $\text{Ni}_{81}\text{Fe}_{19}/\text{Pt}_x\text{Mn}_{1-x}$ bilayer samples with no thermal annealing required. The Pt content of the $\text{Pt}_x\text{Mn}_{1-x}$ films was controlled by adjusting the number of Pt chips on the target and confirmed by energy dispersion X-ray fluorescence (EDXRF) measurements. The unidirectional exchange anisotropy and the uniaxial anisotropy of the exchange coupled $\text{Ni}_{81}\text{Fe}_{19}$ layer were induced by a magnetic field of about 10 Oe in the sputtering chamber during deposition.

A B - H loop tracer with a frequency of 10 Hz was used to characterize the magnetic properties of the films at room temperature. The torque measurements and the blocking temperature measurements were performed on a vibrating sample magnetometer (VSM). A magnetoresistive (MR) probe station was used for resistivity measurements. The crystallographic properties of the thin film samples were determined using X-ray diffraction (XRD). $\theta - 2\theta$ scanning was performed on a Rigaku diffractometer using Cu K_α radiation. Transmission electron microscopy (TEM) was used to examine the microstructures of $\text{Pt}_x\text{Mn}_{1-x}$ films.

3. Results and discussion

3.1. Magnetic properties

Fig. 1 shows the dependence of the exchange field H_e and coercivity H_c of a 25 nm $\text{Ni}_{81}\text{Fe}_{19}$ layer on the thickness of a $\text{Pt}_{10}\text{Mn}_{90}$ layer. Here, the exchange field and coercivity are measured along the easy axis of the $\text{Ni}_{81}\text{Fe}_{19}$ layer. For relatively thick $\text{Pt}_{10}\text{Mn}_{90}$, the exchange field and coercivity remain constant. As the thickness of $\text{Pt}_{10}\text{Mn}_{90}$ layer decreases, the exchange field (and the coercivity) decrease (and increase) rapidly over a narrow $\text{Pt}_{10}\text{Mn}_{90}$ thickness region. For a $\text{Pt}_{10}\text{Mn}_{90}$ thickness less than a certain value, no exchange field is found, and the coercivity decreases to the value of a single $\text{Ni}_{81}\text{Fe}_{19}$ films. Let us define two parameters: the minimum thickness t_{\min} at which the decrease of exchange field starts, and the critical thickness t_{cri} at which the measured exchange field falls to half the value of the maximum exchange field. t_{\min} is important for spin-valve head design, for above this value a well-defined exchange bias can be obtained. t_{cri} was used in Mauri et al.'s paper [11] to characterize the critical thickness effect. We can follow the model described in Ref. [11] to deduce the anisotropy of $\text{Pt}_{10}\text{Mn}_{90}$, which is $12.1 \times 10^5 \text{ erg/cm}^3$.

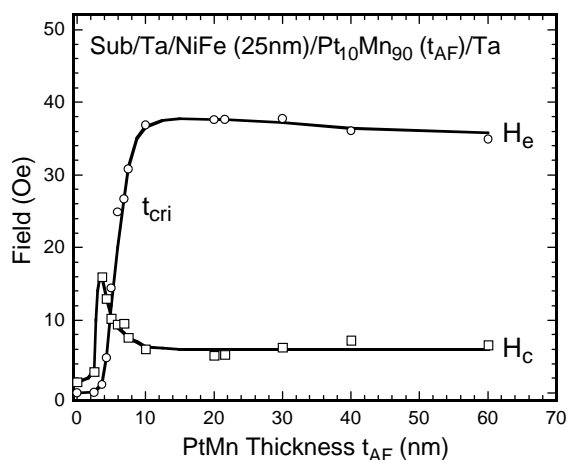


Fig. 1. Antiferromagnetic layer thickness dependence of the exchange field H_e and coercivity H_c in the $\text{Ni}_{81}\text{Fe}_{19}$ (25 nm)/ $\text{Pt}_{10}\text{Mn}_{90}$ bilayer system. The solid lines are guides to the eye.

Fig. 2 shows the variation of the exchange field H_e , the coercivity H_c , and the critical thickness t_{cri} with Pt content for bilayer films with 15 nm $\text{Ni}_{81}\text{Fe}_{19}$. No exchange bias is found for pure Mn films at room temperature. H_e increases with increasing Pt content in the range of 0–8 at%. There is not much change in H_e for samples with Pt content between 8 and 12 at%. H_e decreases with Pt content above 12 at%. From our data, the exchange field with 19 at% Pt content is 16 Oe, just one fourth of the maximum value obtained at 10 at%. An increased coercivity H_c is always observed in the exchange biased FM relative to a single FM film. The coercivity enhancement is larger at the lower Pt content. The critical thickness t_{cri} for the $\text{Ni}_{81}\text{Fe}_{19}$ (25 nm)/ $\text{Pt}_{10}\text{Mn}_{90}$ bilayer system (shown in Fig. 1) is 6 nm. This value

is almost the same as that for $\text{Fe}_{50}\text{Mn}_{50}$ and $\text{Ir}_{20}\text{Mn}_{80}$ [11,12], but is smaller than that for CrMnPt_{10} and $\text{Ni}_{50}\text{Mn}_{50}$ [6,12,13]. Fig. 2(b) shows that the critical thickness and minimum thickness are almost constant within the Pt content region of 4–14 at%. The critical thickness is about 6 nm and the minimum thickness 10 nm. Both the parameters increase rapidly when the Pt content reaches 16 at%. There is no difference in the critical thickness and minimum thickness between $\text{Ni}_{81}\text{Fe}_{19}/\text{Pt}_{10}\text{Mn}_{90}$ samples with 15 nm and 25 nm $\text{Ni}_{81}\text{Fe}_{19}$ films. The exchange bias and coercivity are independent of the FM thickness in the $\text{Ni}_{81}\text{Fe}_{19}/\text{CrMnPt}_x$ ($x=0, 3, 6$ and 9) systems [13] and can be explained by assuming a coherent rotation of the FM magnetization and a short-range exchange coupling at the FM/AF interface.

The AF thickness dependence includes the exchange field, the coercivity, and rotational hysteresis loss, which is related to an irreversible transition of the AF moments [14] and can be used to investigate the mechanism of the exchange bias effect [15]. The energy loss was obtained from torque measurements on samples with 15 nm $\text{Ni}_{81}\text{Fe}_{19}$ deposited on 1 in circular glass substrates. A static magnetic field of 3000 Oe was chosen to saturate the energy loss. Table 1 shows that the torque values are consistent with the values of the unidirectional anisotropy and uniaxial anisotropy obtained from hysteresis loop measurements. However, the magnitudes of both anisotropies are so small that we could not distinguish them from each other in the torque measurements. The energy loss is about 0.2 erg for the sample with thick $\text{Pt}_{10}\text{Mn}_{90}$ layer. For the

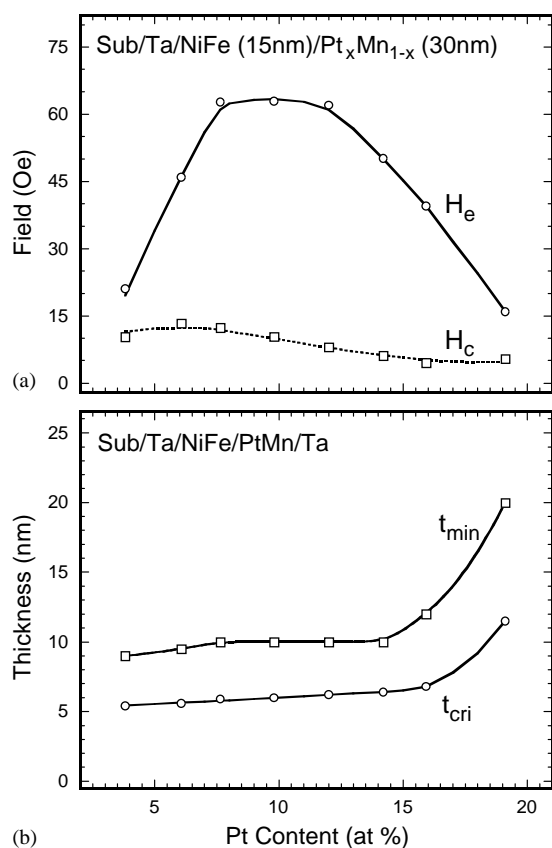


Fig. 2. Exchange field H_e , coercivity H_c , and critical thickness t_{cri} vs. Pt content in the $\text{Ni}_{81}\text{Fe}_{19}$ (15 nm)/ $\text{Pt}_x\text{Mn}_{1-x}$ bilayer system. The lines are guides to the eye.

Table 1

Energy loss from torque measurement for the Sub/Ta (5 nm)/ $\text{Ni}_{81}\text{Fe}_{19}$ (15 nm)/ $\text{Pt}_{10}\text{Mn}_{90}$ (t_{PtMn})/Ta (5 nm) with same dimension (1" circular sample) but different $\text{Pt}_{10}\text{Mn}_{90}$ thickness

| t_{PtMn} (nm) | Peak-peak torque (dyn cm) | Energy loss (erg) |
|------------------------|---------------------------|-------------------|
| 27 | 0.848 | 0.218 |
| 10 | 0.763 | 0.171 |
| 6 | 0.622 | 0.333 |
| 4 | 0.290 | 0.195 |

Pt₁₀Mn₉₀ sample having a critical thickness, 6 nm, the energy loss is about 50% higher than that of thicker Pt₁₀Mn₉₀ samples. The sample with a thinner Pt₁₀Mn₉₀ layer (4 nm in Table 1) shows a smaller energy loss. This AF thickness dependence of the energy loss is also found in other exchange bias systems, such as Ni₈₁Fe₁₉/NiO [16] and Ni₈₁Fe₁₉/CrMnPt_x [6]. Soeya et al. have systematically investigated the effect based on the coherent rotation model of Jacobs and Bean [16].

3.2. Electrical resistivity

The electrical resistivity is strongly correlated to the purity of the material and the perfection of the lattice. Because metallic thin films have more imperfections and lattice strain than bulk materials, the resistivities of these films are higher than the corresponding bulk values and are strongly dependent on the sputtering conditions [17]. Our resistivity measurements were performed on a series of Sub/Ta/Ni₈₁Fe₁₉/Pt_xMn_{1-x}/Ta multilayer samples with different Pt_xMn_{1-x} thicknesses while the thickness of the other layers and the sputtering conditions kept constant. The total sheet resistance, R_{sh} , of the multilayer film is a combination of the sheet resistance of the Pt_xMn_{1-x} layer in parallel with R_{BG} , the background resistance contributed by the electron scattering in the other layers, and at interfaces and surfaces. The resistivity of Pt_xMn_{1-x}, ρ_{PtMn} , is therefore given by the relation,

$$\frac{1}{R_{sh}} = \frac{1}{R_{BG}} + \frac{t_{PtMn}}{\rho_{PtMn}} \quad (1)$$

t_{PtMn} is the thickness of Pt_xMn_{1-x} layer. The sheet resistance of the multilayer films with different Pt_xMn_{1-x} thickness t_{PtMn} is shown in Fig. 3. For a choice of t_{PtMn} thick enough to give an exchange coupling, the total sheet resistance was large enough to obtain reliable resistivity measurements in our MR probe station. From our measurement results shown in Fig. 3, the thickness-dependent total sheet resistances of the multilayer films fit the empirical formula, Eq. (1), well. The resistivity of Pt_xMn_{1-x}, obtained by fitting Eq. (1) to the experimental data, is shown in Fig. 4. A maximum resistivity is found at 10 at% Pt, and then

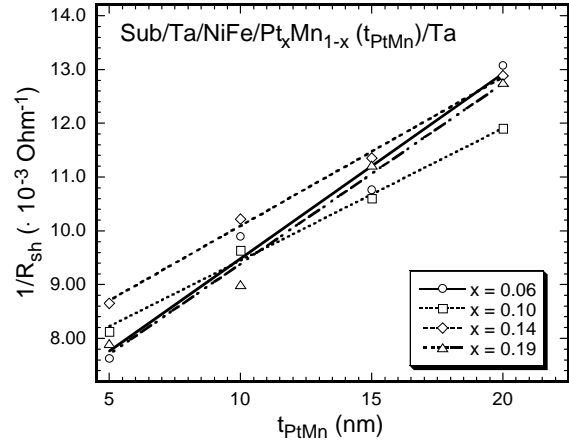


Fig. 3. The total sheet resistance R_{sh} vs. Pt_xMn_{1-x} ($x=6, 10, 14, \text{ and } 19\%$) layer thickness.

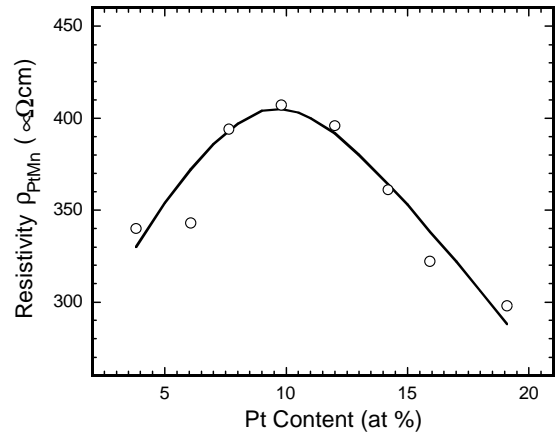


Fig. 4. The Pt content dependence of the resistivity ρ_{PtMn} for the Pt_xMn_{1-x} film deposited on top of the Ni₈₁Fe₁₉ film. The line is guide to the eye.

decreases with increasing Pt content. The overall resistivity of the Pt_xMn_{1-x} is about 350 $\mu\Omega \text{ cm}$. This value is close to the resistivities of Ir₂₀Mn₈₀ and CrMnPt_x, but is significantly greater than those of Fe₅₀Mn₅₀ and Ni₅₀Mn₅₀ [18].

3.3. Thermal effects

The temperature dependence of the exchange field and coercivity was measured using a VSM in a temperature range from room temperature to

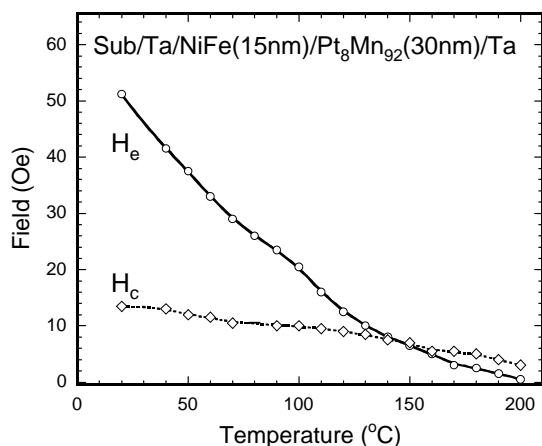


Fig. 5. Exchange field H_e and coercivity H_c vs. temperature for a $\text{Ni}_{81}\text{Fe}_{19}$ (15 nm)/ $\text{Pt}_8\text{Mn}_{92}$ (30 nm) bilayer.

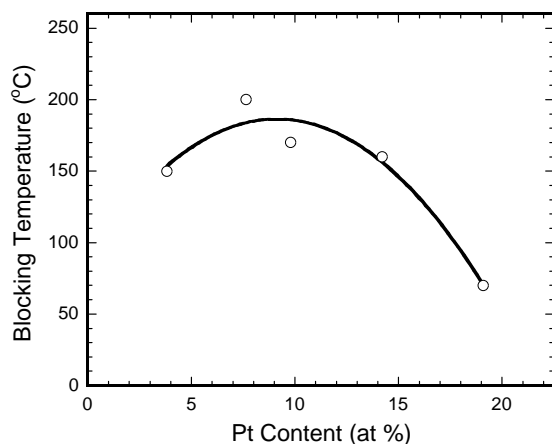


Fig. 6. The Pt content dependence of the blocking temperature. The line is guide to the eye.

200°C. Each measurement cycle took about 30 min. During measurements, the saturation magnetization of the $\text{Ni}_{81}\text{Fe}_{19}$ film decreased less than 10% at high temperature.

Fig. 5 shows representative temperature curves of the exchange field and coercivity in the $\text{Ni}_{81}\text{Fe}_{19}/\text{Pt}_x\text{Mn}_{1-x}$ bilayer system with $x = 8$ at%. Starting from room temperature, the exchange field decreases almost linearly with increasing temperature. The exchange field vanishes at 200°C. The coercivity decreases with increasing temperature in the measurement range.

The blocking temperature T_B is defined as the temperature at which the exchange bias field goes to zero. Fig. 6 shows the dependence of the blocking temperature on the Pt content in $\text{Pt}_x\text{Mn}_{1-x}$ films. The highest blocking temperature is achieved in the $\text{Ni}_{81}\text{Fe}_{19}/\text{Pt}_x\text{Mn}_{1-x}$ bilayer with $x = 8$ at%. Further doping with Pt decreases the blocking temperature. Overall, the blocking temperature for $\text{Ni}_{81}\text{Fe}_{19}$ biased by $\text{Pt}_x\text{Mn}_{1-x}$ is basically the same as that biased by $\text{Fe}_{50}\text{Mn}_{50}$ [19].

3.4. Texture and microstructure

The X-ray diffraction patterns for the $\text{Ni}_{81}\text{Fe}_{19}/\text{Pt}_x\text{Mn}_{1-x}$ ($x = 6, 10, 14,$ and 19 at%) bilayers are shown in Fig. 7. A strong (111) texture for the FCC $\text{Ni}_{81}\text{Fe}_{19}$ was found. $\text{Pt}_x\text{Mn}_{1-x}$ films deposited on the underlying $\text{Ni}_{81}\text{Fe}_{19}$ film were found to

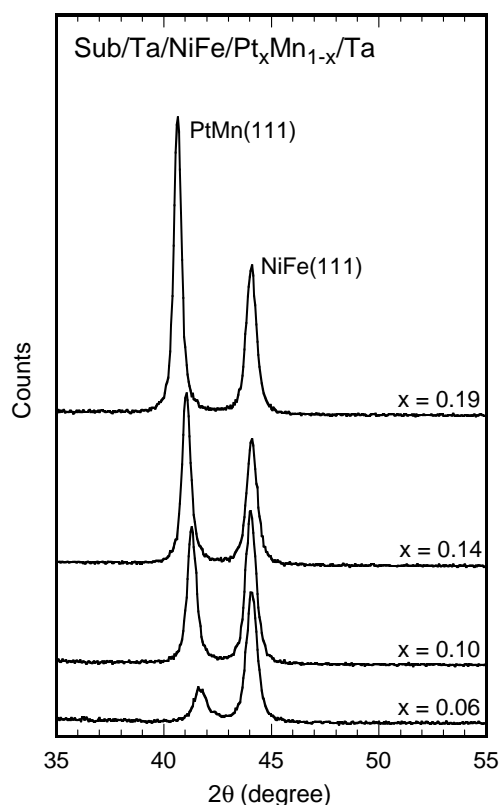


Fig. 7. X-ray diffraction patterns of the $\text{Ni}_{81}\text{Fe}_{19}$ (25 nm)/ $\text{Pt}_x\text{Mn}_{1-x}$ (30 nm) ($x = 6, 10, 14,$ and 19 at%) bilayer films.

have a disordered FCC structure, with the FCC (111) planes growing on the $\text{Ni}_{81}\text{Fe}_{19}$ layer. We see from Fig. 7 that the intensity of the $\text{Pt}_x\text{Mn}_{1-x}$ (111) peak increases with increasing Pt content. The location of the peak moves toward smaller angle, suggesting a lattice expansion in the $\text{Pt}_x\text{Mn}_{1-x}$ films. We estimated the lattice parameter a of the FCC $\text{Pt}_x\text{Mn}_{1-x}$ from Fig. 7. The results are shown in Fig. 8 which shows that a increases linearly with increasing Pt content. The large atomic radius of the Pt causes this increase. The datum for 4 at% Pt deviates from the linear fitting because the $\text{Pt}_4\text{Mn}_{96}$ (111) texture is so weak that the peak location is not easy to pinpoint.

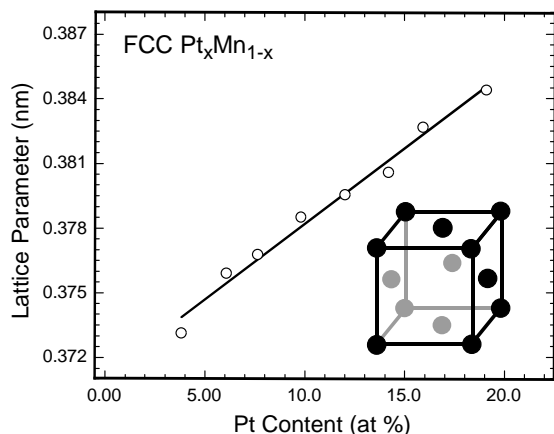


Fig. 8. The Pt content dependence of the lattice parameter a for the FCC $\text{Pt}_x\text{Mn}_{1-x}$ film deposited on top of the $\text{Ni}_{81}\text{Fe}_{19}$ film.

The microstructures of $\text{Ni}_{81}\text{Fe}_{19}/\text{Pt}_x\text{Mn}_{1-x}$ films with x ranging from 4 to 20 at% have been studied by plan view TEM. The measured average grain sizes of $\text{Pt}_x\text{Mn}_{1-x}$ were in the range of 8–11 nm, increasing slightly with Pt composition. From electron diffraction determination, it was found that γ -PtMn with a disordered FCC structure was the dominant phase in the $\text{Pt}_x\text{Mn}_{1-x}$ films. The γ -PtMn grains were (111)-textured in the film plane. Fig. 9 shows the TEM images and corresponding electron diffraction patterns of $\text{Pt}_{10}\text{Mn}_{90}$ (a) and $\text{Ni}_{81}\text{Fe}_{19}/\text{Pt}_{10}\text{Mn}_{90}$ (b) films. The $\text{Pt}_{10}\text{Mn}_{90}$ grains in Fig. 9(a) have clear grain boundaries. The strong intensity of the (220) diffraction ring in Fig. 9(a) indicates that $\text{Pt}_x\text{Mn}_{1-x}$ grains are (111)-textured. From dark field TEM images taken by applying (111) and (220) diffraction rings, it was found that some random oriented $\text{Pt}_x\text{Mn}_{1-x}$ clusters existed in the $\text{Pt}_x\text{Mn}_{1-x}$ layers and (111) textured $\text{Pt}_x\text{Mn}_{1-x}$ grains had comparably larger grain size. Many Moiré fringes with the same fringe distance can be seen in Fig. 9(b). The moiré fringes are due to the interference of overlapped (220) planes of $\text{Ni}_{81}\text{Fe}_{19}$ and $\text{Pt}_x\text{Mn}_{1-x}$ grains. The existence of many Moiré fringes with the same fringe distance implies good texture of both $\text{Ni}_{81}\text{Fe}_{19}$ and $\text{Pt}_x\text{Mn}_{1-x}$ grains. This result is also confirmed by the strong (220) diffraction rings of the $\text{Ni}_{81}\text{Fe}_{19}$ and the $\text{Pt}_x\text{Mn}_{1-x}$ in Fig. 9(b). Since we could not see the (111) diffraction ring of $\text{Ni}_{81}\text{Fe}_{19}$ in Fig. 9(b), the $\text{Ni}_{81}\text{Fe}_{19}$ grains had much less random oriented component than that of $\text{Pt}_x\text{Mn}_{1-x}$.

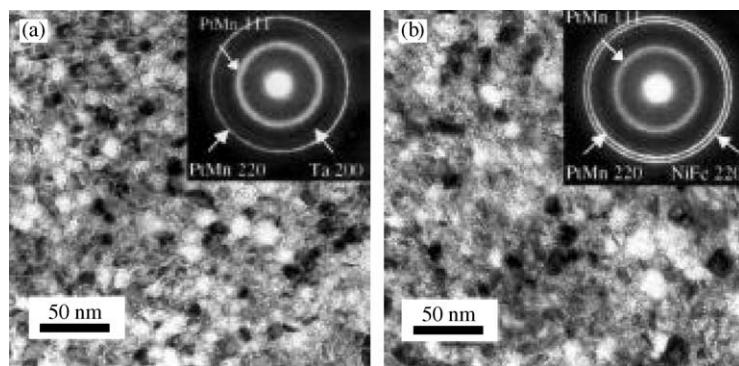


Fig. 9. Bright field images of plan view TEM and electron diffraction for (a) the $\text{Pt}_{10}\text{Mn}_{90}$ single layer and (b) the $\text{Ni}_{81}\text{Fe}_{19}/\text{Pt}_{10}\text{Mn}_{90}$ layer in the glass/Ta (5 nm)/ $\text{Ni}_{81}\text{Fe}_{19}$ (15 nm)/ $\text{Pt}_{10}\text{Mn}_{90}$ (30 nm)/Ta (5 nm) sample.

Usually a thin amorphous Ta buffer layer is first deposited on glass to promote the (1 1 1) texture of the $\text{Ni}_{81}\text{Fe}_{19}$ layer that grows on top of it. We have made a series of $\text{Ta}/\text{Ni}_{81}\text{Fe}_{19}$ (15 nm)/ $\text{Pt}_{16}\text{Mn}_{84}$ (30 nm)/Ta (5 nm) samples with different Ta underlayer thickness. The XRD patterns show that no textures of the $\text{Ni}_{81}\text{Fe}_{19}$ layer and $\text{Pt}_{16}\text{Mn}_{84}$ layer was found (see Fig. 10) in the sample without a Ta underlayer. Strong $\text{Ni}_{81}\text{Fe}_{19}$ (1 1 1) and $\text{Pt}_{16}\text{Mn}_{84}$ (1 1 1) textures appear when the Ta underlayer is amorphous and just 2.5 nm thick. The Ta underlayer crystallizes as its thickness reaches 10 nm and the phase is identified as a tetragonal β -Ta. The β -phase is often nucleated on substrates having a surface oxide such as glass or quartz [20]. With increasing Ta thickness, the β -Ta texture with (002) orientation as well as (3 3 0)

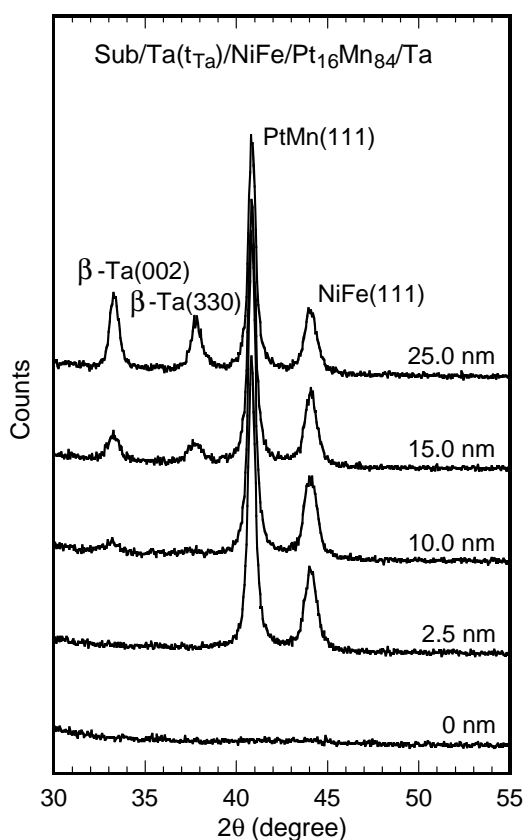


Fig. 10. X-ray diffraction patterns of the $\text{Ni}_{81}\text{Fe}_{19}$ (15 nm)/ $\text{Pt}_{16}\text{Mn}_{84}$ (30 nm) films with Ta underlayer thickness of 0, 2.5, 10, 15 and 25 nm.

Table 2

Exchange field H_e and coercivity H_c of the $\text{Sub}/\text{Ta}/\text{Ni}_{81}\text{Fe}_{19}$ (15 nm)/ $\text{Pt}_{16}\text{Mn}_{84}$ (30 nm)/Ta (5 nm) with different Ta underlayer thickness

| Ta underlayer thickness (nm) | H_e (Oe) | H_c (Oe) |
|------------------------------|------------|------------|
| 0 | 0.3 | 0.9 |
| 2.5 | 37.3 | 5.51 |
| 5 | 39.5 | 4.50 |
| 10 | 39.0 | 5.73 |
| 15 | 37.8 | 4.85 |
| 25 | 38.5 | 5.61 |

orientation becomes stronger. However, we have not seen the reduction of the $\text{Ni}_{81}\text{Fe}_{19}$ (1 1 1) and $\text{Pt}_{16}\text{Mn}_{84}$ (1 1 1) textures associated with the crystallization of the multi-oriented Ta underlayer. The FM and AF textures play important roles in the exchange bias between the $\text{Ni}_{81}\text{Fe}_{19}$ and $\text{Pt}_{16}\text{Mn}_{84}$ films. As Table 2 shows, the exchange field and coercivity are similar for the samples with Ta underlayers, but no exchange bias was found in the sample without a Ta underlayer as a result of the non-textured $\text{Ni}_{81}\text{Fe}_{19}$ and $\text{Pt}_{16}\text{Mn}_{84}$ films.

3.5. Discussion

An early study [21] of bulk $\text{Pt}_x\text{Mn}_{1-x}$ showed that the ordered PtMn_3 , with a γ' -PtMn phase having a type of Cu_3Au structure, had a Néel temperature of 475°K, i.e., $\sim 200^\circ\text{C}$. However, this result might not be applicable to our $\text{Pt}_x\text{Mn}_{1-x}$ thin films. It is known that the γ -phase for pure Mn with the FCC structure is only stable between 1079 and 1140 K, but the γ -phase can be produced by doping with other elements at room temperature [22–25]. From electron diffraction of the samples that we investigated, the disordered FCC γ -PtMn phase dominates the $\text{Pt}_x\text{Mn}_{1-x}$ films. In the samples with a small amount of Pt doping (e.g., 6 at%) an α -Mn phase was also found. Although the γ' -PtMn phase was found in samples with relatively high Pt content, its amount was remarkably less than that of the γ -PtMn. In addition, large $\text{Pt}_x\text{Mn}_{1-x}$ grains were found to be composed mainly of the γ -PtMn.

The reported Néel temperatures for bulk γ -TMn ($T = \text{Fe}, \text{Ni}, \text{Zn}, \text{Cu}$) was less than 500 K [22–25].

In addition, the magnetic moment and Néel temperature were experimentally found to decrease with the dopant concentration. Although exchange biasing is an interfacial exchange effect, the pinning of the FM layer requires a well-ordered AF film in contact with it. Therefore, the blocking temperature of an exchange coupled AF/FM bilayer will generally be less than the Néel temperature of the AF film. Consequently in our $\text{Ni}_{81}\text{Fe}_{19}/\text{Pt}_x\text{Mn}_{1-x}$ system, at high Pt content, decrease of the blocking temperature with increasing Pt content we take to be associated with a decreasing Néel temperature of the $\text{Pt}_x\text{Mn}_{1-x}$ with Pt doping. The “tail” of the temperature curve of the exchange field near the blocking temperature shown in Fig. 5 suggests a dispersion of $\text{Pt}_x\text{Mn}_{1-x}$ grain size, in which large grains have a higher Néel temperature [26–27]. For the samples with low Pt content, the $\text{Pt}_x\text{Mn}_{1-x}$ layer is composed of γ -PtMn as well as α -Mn, and the grains are relatively small. This results in a low blocking temperature.

The dependences of the exchange field and coercivity on $\text{Pt}_x\text{Mn}_{1-x}$ film composition are consistent with that of the blocking temperature. From the point of view of a polycrystalline grain model [28], the exchange bias arises from the FM/AF interfacial exchange coupling, and is strongly dependent on the intrinsic properties of the antiferromagnetic grains, such as the exchange coupling between the AF moments and their magnetocrystalline anisotropies. Strong AF-moment coupling and large AF magnetocrystalline anisotropy contribute to a large exchange bias. Although the γ -PtMn (111) texture improves with increasing of Pt content, the exchange coupling constant A_{AF} and the anisotropy K_{AF} at room temperature of $\text{Pt}_x\text{Mn}_{1-x}$ presumably decrease with the dopant content since the blocking temperature decreases with the Pt content. The decrease of the AF magnetocrystalline anisotropy with the Pt content is consistent with the behavior of the minimum AF thickness t_{min} required for the exchange bias (see Fig. 2). An exchange-biased system with a small exchange field but a large t_{min} suggests a small anisotropy for the AF layer [11,13].

This argument may not be suitable for the exchange-biased bilayers with low Pt content, in

which a small exchange anisotropy is observed. Since the $\text{Pt}_x\text{Mn}_{1-x}$ film is neither well-textured nor well-crystallized, the exchange bias is affected by both the resulting complicated interfacial coupling and the degraded intrinsic properties of the AF film. The large coercivity at low Pt content could be associated with non-ideal aspects of the film as well. We notice that the $\text{Pt}_x\text{Mn}_{1-x}$ grains in the film with low Pt content are also smaller, and are therefore easier to undergo irreversible motion during the FM magnetization reversal, resulting in an enhancement of coercivity [15].

4. Summary

Based on our studies of $\text{Ni}_{81}\text{Fe}_{19}/\text{Pt}_x\text{Mn}_{1-x}$ ($0 < x < 20$ at%) bilayers, $\text{Pt}_x\text{Mn}_{1-x}$, as an exchange biasing material, shows properties similar to $\text{Fe}_{50}\text{Mn}_{50}$ and $\text{Ir}_{20}\text{Mn}_{80}$ [11,18]. Compared with γ - $\text{Fe}_{50}\text{Mn}_{50}$, $\text{Pt}_x\text{Mn}_{1-x}$ has almost the same exchange field and blocking temperature, a slightly larger minimum thickness, but remarkably larger resistivity. The similarity is reasonable because the γ -phases of Mn-based binary alloys contribute to the exchange bias. Besides, the dependence of the exchange bias in $\text{Ni}_{81}\text{Fe}_{19}/\text{Pt}_x\text{Mn}_{1-x}$ bilayers on the $\text{Pt}_x\text{Mn}_{1-x}$ composition can be understood by the intrinsic properties of the γ -phase, which varies with the Pt content.

Acknowledgements

This work was supported by the National Science Foundation under Grant No. ECD-8907068. One of the authors, (H.X.), would like to thank Dr. Pei Zou and Dr. Fabian Lee for technical assistance.

References

- [1] R.D. Hempstead, S. Krongelb, D.A. Thompson, IEEE Trans. Magn. 14 (1978) 521.
- [2] M. Carey, A.E. Berkowitz, Appl. Phys. Lett. 60 (1992) 3060.
- [3] T. Lin, D. Mauri, N. Staud, C. Hwang, J.K. Howard, G.L. Gorman, Appl. Phys. Lett. 65 (1994) 1183.

- [4] M. Konoto, M. Tsunoda, M. Takahashi, *J. Appl. Phys.* 85 (1999) 4925.
- [5] R. Nakatani, H. Horoyuki, K. Hoshino, Y. Sugita, *J. Magn. Magn. Mater.* 173 (1997) 321.
- [6] S. Soeya, H. Hoshiya, M. Fuyama, S. Tadokoro, *J. Appl. Phys.* 80 (1996) 1006.
- [7] H. Xi, R.M. White, *J. Appl. Phys.* 87 (2000) 410.
- [8] S. Araki, E. Omata, M. Sano, M. Ohta, K. Noguchi, H. Morita, M. Matsuzaki, *IEEE Trans. Magn.* 34 (1998) 387.
- [9] M. Saito, Y. Kakaiharu, T. Watanabe, N. Hasegawa, *J. Magn. Soc. Japan* 21 (1997) 505.
- [10] H. Xi, B. Bian, D.E. Laughlin, R.M. White, *J. Appl. Phys.* 87 (2000) 4918.
- [11] D. Mauri, E. Kay, D. Scholl, J.K. Howard, *J. Appl. Phys.* 62 (1987) 2929.
- [12] A.J. Devasahayam, *Biasing materials for anisotropic magnetoresistive and spin-valve heads*, Ph.D. thesis, Carnegie Mellon University, Pittsburgh, 1998.
- [13] H. Xi, R.M. White, *Phys. Rev. B* 61 (2000) 1318.
- [14] L. Néel, in: N. Kurti (Ed.), *Selected Works of Louis Néel*, Gordon and Breach, New York, 1988.
- [15] H. Xi, R.M. White, *Phys. Rev. B* 61 (2000) 80.
- [16] S. Soeya, S. Nakamura, T. Imagawa, S. Narishige, *J. Appl. Phys.* 77 (1995) 5838.
- [17] M. Ohring, *The Materials Science of Thin Films*, Academic Press, San Diego, 1992.
- [18] M. Lederman, *IEEE Trans. Magn.* 35 (1999) 794.
- [19] C. Tsang, K. Lee, *J. Appl. Phys.* 53 (1982) 2605.
- [20] W.D. Westwood, N. Waterhouse, P.S. Wilcox, *Tantalum Thin Films*, Academic Press, London, 1975.
- [21] E. Krén, G. Kádár, L. Pál, J. Sólyom, P. Szabó, T. Tarnóczy, *Phys. Rev.* 171 (1968) 574.
- [22] D. Meneghetti, S.S. Sidhu, *Phys. Rev.* 105 (1957) 130.
- [23] Y. Endoh, Y. Ishikawa, *J. Phys. Soc. Japan* 30 (1971) 1614.
- [24] H. Uchishiba, *J. Phys. Soc. Japan* 31 (1971) 436.
- [25] N. Honda, Y. Tanji, Y. Nakagawa, *J. Phys. Soc. Japan* 41 (1976) 1931.
- [26] H.N. Fuke, K. Saito, M. Yoshikawa, H. Iwasaki, M. Sahashi, *Appl. Phys. Lett.* 75 (1999) 3680.
- [27] H. Xi, *Study of exchange bias for magnetoelectronic sensors*, Ph.D. dissertation, Carnegie Mellon University, Pittsburgh, 2001.
- [28] M.D. Stiles, R.D. McMichael, *Phys. Rev. B* 59 (1999) 3722.